

Automatic Detection and Correction Algorithms for Magnetic Saturation in the SMFT/HSOS longitudinal Magnetograms

*Hai-qing, Xu¹, Suo Liu¹, *Jiang-tao Su^{1,2}, Yuan-yong Deng^{1,2}, Andrei Plotnikov³, Xian-yong Bai^{1,2}, Jie Chen¹, Xiao Yang¹, Jing-jing Guo¹, Xiao-fan Wang¹ and Yong-liang Song¹

¹ Key Laboratory of Solar Activity, National Astronomical Observatories, Chinese Academy of Sciences, Beijing, 100101, China; *xhq@bao.ac.cn*; *sjt@bao.ac.cn*

² School of Astronomy and Space Sciences, University of Chinese Academy of Sciences, 19 A Yuquan Road, Shijingshan District, Beijing 100049, China

³ Crimean Astrophysical Observatory, Russian Academy of Sciences, Nauchny, Crimea, 298409, Russia

Received 20xx month day; accepted 20xx month day

Abstract longitudinal magnetic field often suffers the saturation effect in strong magnetic field region when the measurement performs in a single-wavelength point and linear calibration is adopted. In this study, we develop a method **that** can judge the threshold of saturation in Stokes V/I observed by the Solar Magnetic Field Telescope (SMFT) and **correct for** it automatically. **The procedure is that** first perform the second-order polynomial fit to the Stokes V/I vs I/I_m (I_m is the maximum value of Stokes I) curve to estimate the threshold of saturation, then reconstruct Stokes V/I in strong field region to **correct for** saturation. The algorithm is proved to be effective by comparing with the magnetograms obtained by the Helioseismic and Magnetic Imager (HMI). The accurate rate of detection and correction for saturation is $\sim 99.4\%$ and $\sim 88\%$ respectively among 175 active regions. The advantages and disadvantages of the algorithm are discussed.

Key words: Sun: sunspots — Sun: magnetic field — Methods: data analysis

1 INTRODUCTION

The study of solar magnetic field has always been a core topic in solar physics. Some major unsolved scientific problems in the study of solar physics, such as the generation of solar cycle, coronal heating, the origin of solar eruptions and so on, are all related to the solar magnetic field. The magnetic field of sunspots was first investigated by [Hale \(1908\)](#). It is known that **generally**, the present magnetographs measure solar polarized light (present as Stokes parameters I , Q , U , and V) rather than magnetic fields. Under a certain atmospheric models and assumptions, the solar magnetic field is obtained **through** inver-

and many interesting results have been presented from these observations. **Yet**, there are still some basic questions on the measurements of solar magnetic fields **waiting** to be carefully analyzed (Zhang 2019). Svalgaard et al. (1978) found the magnetograph was saturated when magnetic field is very strong. Ulrich et al. (2002) discussed reasons and treatment of saturation effects in the Mount Wilson 150 foot tower telescope system in detail. They pointed out that most spectral lines used for magnetic measurements are subject to this saturation effect for at least some parts of their profile. Liu et al. (2007) found another type of saturation in sunspot umbrae observed by the Michelson Doppler Imager on the Solar and Heliospheric Observatory (MDI/SOHO) caused by the 15-bit on-board numerical treatment used in deriving the MDI magnetograms. The saturation effect can be eliminated by using the information on spectral line, e.g., the Spectro-polarimeter (SP) onboard Hinode (Kosugi et al. 2007) obtains spectral profile with a wide spectral range, and the Helioseismic and Magnetic Imager on board the Solar Dynamics Observatory (HMI/SDO, Schou et al. 2012) obtains spectral profile with six wavelength points. The saturation effect needs to be **corrected** by some supplementary methods if the polarized light is measured in a single-wavelength point and linear calibration is adopted. Chae et al. (2007) performed cross-calibration of Narrow-band Filter Imager (NFI) Stokes V/I and longitudinal magnetic field acquired by the SP, and proposed to use two different linear relationships of longitudinal magnetic field and Stokes V/I from Hinode/NFI to **correct for saturation**. Moon et al. (2007) used a pair of MDI intensity and magnetogram data simultaneously observed, and the relationship from the cross-comparison between the SP and MDI flux densities to **correct for saturation** in magnetic field obtained by MDI. Guo et al. (2020) explored a nonlinear calibration method to deal with the saturation problem, which used a multilayer perceptron network.

The Solar Magnetic Field Telescope (SMFT) at the Huairou Solar Observing Station (HSOS) of the National Astronomical Observatories of China is a 35 cm vacuum telescope equipped with a birefringent filter for wavelength selection and KD*P crystals to modulate polarization signals. The Fe I 5324.19 Å line is used for measurements. A vector magnetogram is built using four narrow-band (0.125 Å) Stokes I, Q, U and V maps. The center wavelength of the filter can be tuned and is normally at -0.075 Å for the measurements of longitudinal magnetic fields and at the line center for the transversal magnetic fields (Ai & Hu 1986). It has been observing vector magnetic fields for more than 30 years. The theoretical calibration for SMFT vector magnetogram was first made by Ai et al. (1982). Several different methods of the magnetic field calibration under the weak-field assumption have been done since then. Wang et al. (1996) used an empirical calibration and a velocity calibration methods to calibrate the longitudinal magnetograms. Su & Zhang (2004) used 31 points of the Fe I 5324.19 Å spectral line profile to derive vector magnetic field by non-linear least squares fitting technique. Bai et al. (2014) improved the calibration process by fitting the observed full Stokes information using six points of the profile of Fe I 5324.19 Å line, and the analytical Stokes profiles under the Milne-Eddington atmosphere model, adopting the Levenberg-Marquardt least-squares fitting algorithm. However, the routine measurements of Stokes I, Q, U and V parameters by SMFT are being performed in a single-wavelength point. The longitudinal magnetic field is reconstructed by equation 1:

where C_L is the calibration coefficient inferred from the aforementioned calibration methods. This linear calibration will result in the saturation when magnetic field is strong. Plotnikov et al. (2019) made an attempt to improve the routine magnetic field measurements of SMFT by introducing non-linear relationship between the Stokes V/I and longitudinal magnetic field. They performed cross-calibration of SMFT data and magnetograms provided by HMI to determine the form of the relationship. They found that the magnetic field saturation inside sunspot umbra can be eliminated by using non-linear relationship between Stokes V/I and longitudinal magnetic field. They also discussed the influence of saturation effect **on solving the 180 degree ambiguity** of the transversal magnetic field. They manually chose the threshold for separating pixels into two subsets of strong and weak magnetic field, which is not convenient for dealing with large data sample.

In this paper, we attempt to develop a method which can judge the threshold of saturation in SMFT longitudinal field and **correct for** saturation automatically. One purpose of this study is to **correct for saturation** in longitudinal magnetic field obtained by SMFT since 1987. Another purpose is to prepare calibration technique for the Full-disk vector MagnetoGraph (FMG, Deng et al. 2019) which is one payload **onboard** the Advanced Space-based Solar Observatory (ASO-S, Gan et al. 2019) that will be launched in early 2022. The routine observations for the FMG will be taken at one wavelength position of the Fe I 5324.179 Å (Su et al. 2019). The magnetic field will be suffered saturation effect if the linear calibration is adopted.

2 OBSERVATIONS

The raw data registered by SMFT **are** left and right polarized light. The Stokes V/I and I are calculated as following:

$$\begin{aligned}\frac{V}{I} &= \frac{V_l - V_r}{V_l + V_r} \\ I &= V_l + V_r\end{aligned}\tag{2}$$

where $V_l = \frac{I+V}{2}$ and $V_r = \frac{I-V}{2}$ represent modulated filtergrams. After this process, the influence of flat field is eliminated. The pixel size of SMFT data is approximately $0.29'' \times 0.29''$ since 2012 and the **spatial** resolution is approximately $2''$ produced by local seeing effect. We selected 9 active regions (AR) in between 2013 and 2015 for case study and 175 ARs in 2013 for statistical study. The data were performed **by** 4×4 pixels median filtering to reduce the noise.

To check the effectiveness of correction method for saturation, we downloaded the co-temporal magnetograms of the selected 9 ARs from HMI/SDO. HMI is a full-disk filtergraph that measures the profile of photospheric Fe I 6173 Å line at six wavelength positions in two polarization states to derive the longitudinal magnetic field. The spatial resolution of the instrument is $1''$ with $0.5'' \times 0.5''$ pixel size. In order to perform a detailed pixel by pixel comparison, **HMI magnetograms** were rotated for the p -angle correction and reduced **in** spatial resolution to $2''$ by a 2-D Gauss-smooth function. Both data are re-scaled to the pixel size of $0.5'' \times 0.5''$. Then the same region **that** includes the maximized size of sunspots are selected and

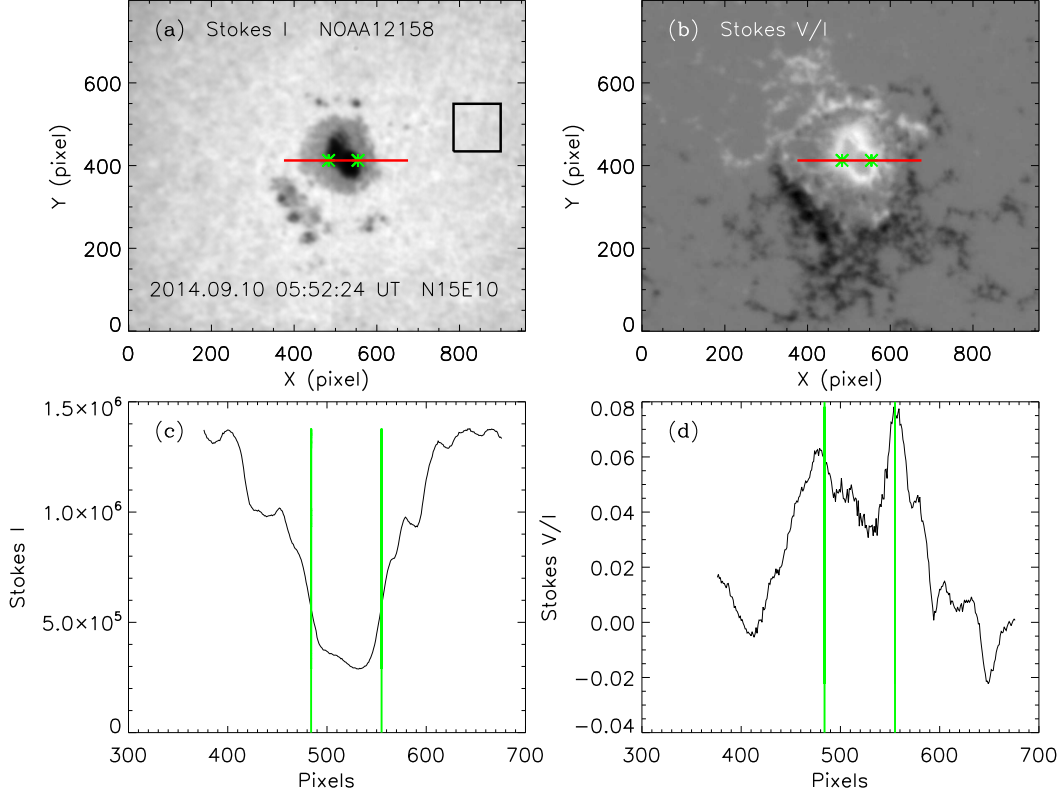


Fig. 1: Panels (a) and (b) are maps of Stokes I and V/I observed on 2014 September 10 by SMFT. The rectangle region in panel (a) is used to calculate I_c . Panels (c) and (d) show the distribution of Stokes I and V/I along the red line; The green lines indicate the saturation locations marked by asterisks.

3 METHOD

The studies show that there is a relationship between the continuum intensity and magnetic field, and the smallest intensity always corresponding to the largest magnetic field (*e.g.*, [Martínez & Vázquez 1993](#); [Norton & Gilman 2004](#); [Leonard & Choudhary 2008](#)). Figure 1(a) and (b) show the maps of Stokes I and V/I for active region NOAA12158 observed on 2014 September 10 by SMFT. Figure 1(c) and (d) show the distribution of Stokes I and V/I along the red line. The Stokes I decreases to the minimum in the sunspot center, but the Stokes V/I stops increasing at the points marked by green lines (asterisks) corresponding to sunspot umbrae. This phenomenon is called magnetic saturation. If **performing** linear calibration, the longitudinal magnetic field will **get weakened** in sunspot umbrae **in comparing with its surrounding area**.

Next, we will show two examples to give a detail description for the detection and correction method for saturation effect.

3.1 Detection Algorithm for Magnetic Saturation

The relationship between $|V/I|$ and I/I_c (I/I_m) for NOAA12158 is given in Figure 2(a) ((b)). I_c is the

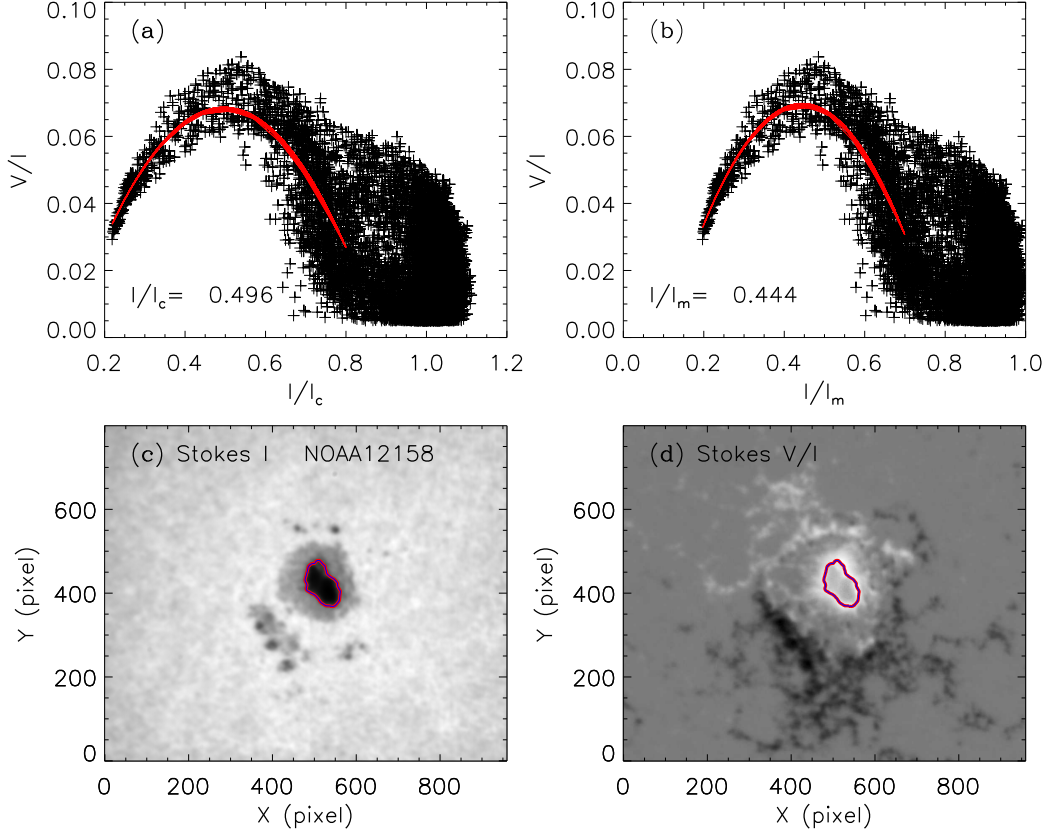


Fig. 2: Scatter plots of $|V/I|$ vs I/I_c (panel (a)) and I/I_m (panel (b)) for NOAA12158. The red line is the best-fit second-order polynomial and I/I_c (I/I_m) marked in panel is corresponding to the apex. The red and blue contours in panels (c) and (d) represent $I/I_c=0.496$ and $I/I_m=0.444$. V/I uses the absolute values in the plots, similarly hereinafter.

I within the whole active region. $|V/I|$ first increases with Stokes I decreasing (going to sunspot center), then decreases. It is found that the second-order polynomial (red line) gives a well fit when $|V/I| > 0.02$ and $I/I_c \leq 0.8$ ($I/I_m \leq 0.7$). Moon et al. (2007) found similar relationship between MDI flux density and intensity **in magnetic saturation regions**, and used the second-order polynomial to separate the strong and weak field area. The pixels are separated into two parts by the apex. It is easy to calculate coordinates of the apex by fitting coefficient. We find that the corresponding I/I_c is 0.496 and I/I_m is 0.444, which are denoted in Figure 2(c) and (d) by blue and red contours. Although the value of I/I_c and I/I_m is different, the region in Stokes I and $|V/I|$ maps is the same. When $I/I_c < 0.496$ ($I/I_m < 0.444$), it is corresponding to the sunspot umbrae where the $|V/I|$ suffered from saturation. So we may use this value as the threshold to detect **the saturation regions** in longitudinal magnetic field.

We performed the same analysis for NOAA12305 which includes multiple sunspots. We used the observation on 2015 Mar 27. The similar relationship was found between $|V/I|$ and I/I_c (I/I_m) as NOAA12158 when $|V/I| > 0.02$ and $I/I_c \leq 0.8$ ($I/I_m \leq 0.75$). The I/I_c (I/I_m) is 0.577 (0.529) corresponding to the apex of the second-order polynomial (red line in Figure 3(a) and (b)), which are denoted in Figure 3(c) and

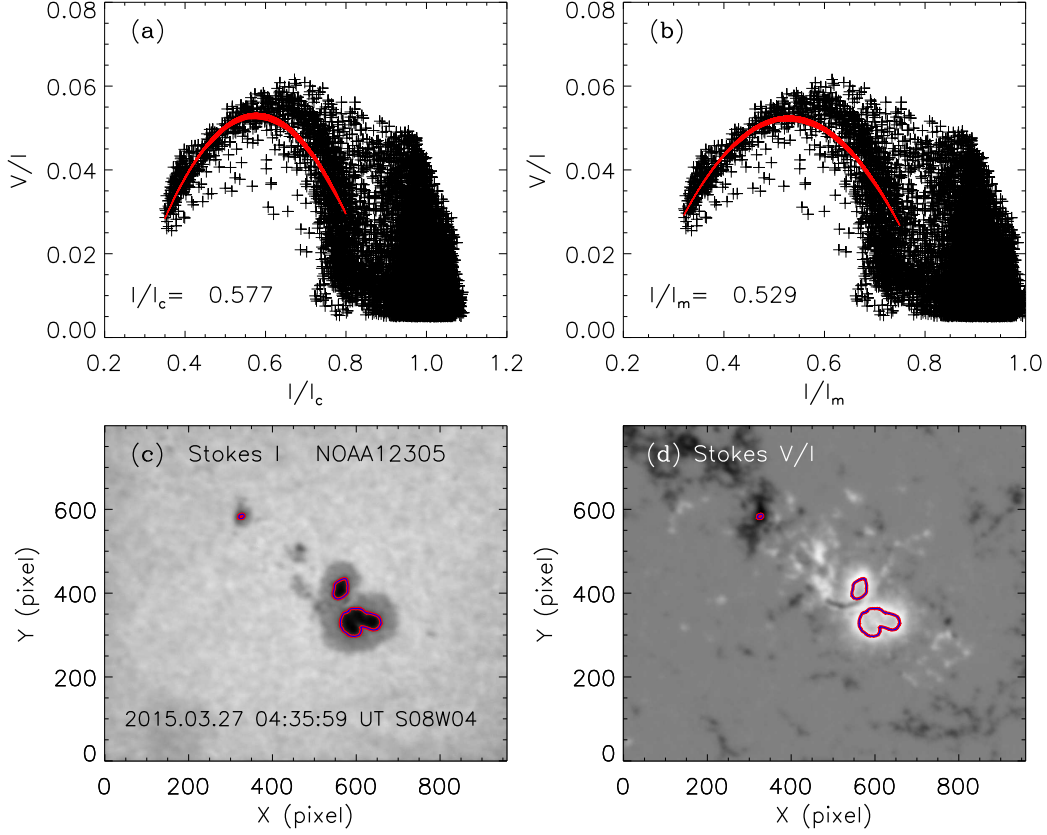


Fig. 3: Similar as Figure 2, but for NOAA12305.

Table 1: Threshold of detecting magnetic saturation for 9 ARs observed by SMFT

NOAA	Date	Position	I/I_c	I/I_m
11658	2013.11.19	S11W10	0.602	0.497
11899	2013.11.16	N06W03	0.420	0.382
11960	2014.01.25	S14E01	0.661	0.585
12027	2014.06.07	N13W01	0.579	0.492
12055	2014.05.12	N10W02	0.664	0.557
12149	2014.08.27	N10E11	0.543	0.472
12158	2014.09.10	N15E10	0.496	0.444
12305	2015.03.27	S08W04	0.577	0.529
12325	2015.04.19	N04E02	0.638	0.582

We listed the thresholds for detecting saturation obtained by the above method for 9 active regions in Table 1. It can be seen that the thresholds are different for each active region. So it is necessary to calculate the threshold for individual active region. There is no difference in detecting the saturation region using

3.2 Correction Algorithm for Magnetic Saturation

We take the above two active regions as examples to show how to correct saturation effect. We re-plot $|V/I|$ vs I/I_m in Figure 4. The correction procedure for magnetic saturation is as following:

- (1) The threshold I_0 for occurrence of magnetic saturation is determined by the above algorithm, which corresponds to green asterisks in Figure 4(a) and (d).
- (2) The pixels are separated into two parts by threshold I_0 . **Those with $I/I_m < I_0$ are suffered from saturation effect. Both linear (green lines in Figure 4(b) and (e)) and the second-order polynomial functions (yellow lines in Figure 4(b) and (e)) are used to fit the scatter plots for saturation data. The green and yellow lines almost overlap. For its simplicity, we finally choose the linear functions to fit the scatter plots for both saturation and good data.** The fitting coefficients are (a_1, c_1) and (a_2, c_2) corresponding to green and blue lines in Figure 4(b) and (e), respectively. a_1 and a_2 are slopes, c_1 and c_2 are constants. Using equation 3 to calculate Stokes V/I for pixels where $I/I_m < I_0$,

$$\frac{V^s}{I} = \left| \frac{a_2}{a_1} \left(\left| \frac{V}{I} \right| - c_1 \right) + c_2 \right| \cdot \text{sign} \left(\frac{V}{I} \right). \quad (3)$$

- (3) After re-calculating, the Stokes V/I maps are shown in Figure 5(a) and (c). It can be seen that the saturation in sunspot umbrae has been eliminated. But the discontinuity at the boundary of umbrae and penumbrae can be seen. To eliminate this discontinuity, we calculate the $\pm 1\sigma$ uncertainty of I_0 corresponding to the cyan ($I_{+\sigma}$) and blue ($I_{-\sigma}$) asterisks in Figure 4(a) and (d). For pixels where $I_{-\sigma} < I/I_m < I_{+\sigma}$, V/I is calculated by interpolation. Then smooth the data by Gauss-smooth function. The new V/I maps are shown in Figure 5(b) and (d). It can be seen that the discontinuity has been eliminated. The scatter plots of $|V/I|$ vs I/I_m are shown in Figure 4(c) and (f). The relationship is approximate linear.

4 COMPARISON BETWEEN SMFT AND HMI DATA

The SMFT longitudinal magnetic field B_L^{SMFT} can be re-calibrated from equation 4:

$$B_L^{SMFT} = \begin{cases} C_L \frac{V^s}{I} , & \frac{I}{I_m} < I_0 \\ C_L \frac{V}{I} , & \frac{I}{I_m} \geq I_0 \end{cases} \quad (4)$$

where C_L is calibration coefficient. We adopt 8381 G as proposed by Su & Zhang (2004).

The comparison of longitudinal magnetic field observed by SMFT and HMI for NOAA12158 is shown in Figure 6. It can be seen that the distribution of B_L^{SMFT} and HMI longitudinal magnetic field B_L^{HMI} is very similar (Figure 6(a) and (b)). The scatter plots of B_L^{SMFT} and B_L^{HMI} before and after correcting saturation effect are shown in Figure 6(c) and (d), respectively. The B_L^{SMFT} starts to decrease when B_L^{HMI} is larger than 1300 G before correcting saturation effect. The linear correlation coefficient is 0.86. After correcting saturation effect in B_L^{SMFT} , the relationship of B_L^{SMFT} and B_L^{HMI} is closer to linear. The linear correlation coefficient increases to 0.96. Such good correlation indicates that the proposed correction method for saturation in B_L^{SMFT} is effective for this active region.

Figure 7 shows the comparison of B_L^{SMFT} and B_L^{HMI} for NOAA12305. It is also found that the B_L^{SMFT} starts to decrease when B_L^{HMI} is larger than 1300 G before correcting saturation effect. The linear correlation coefficient is 0.88. After correcting saturation effect in B_L^{SMFT} , a good correlation be-

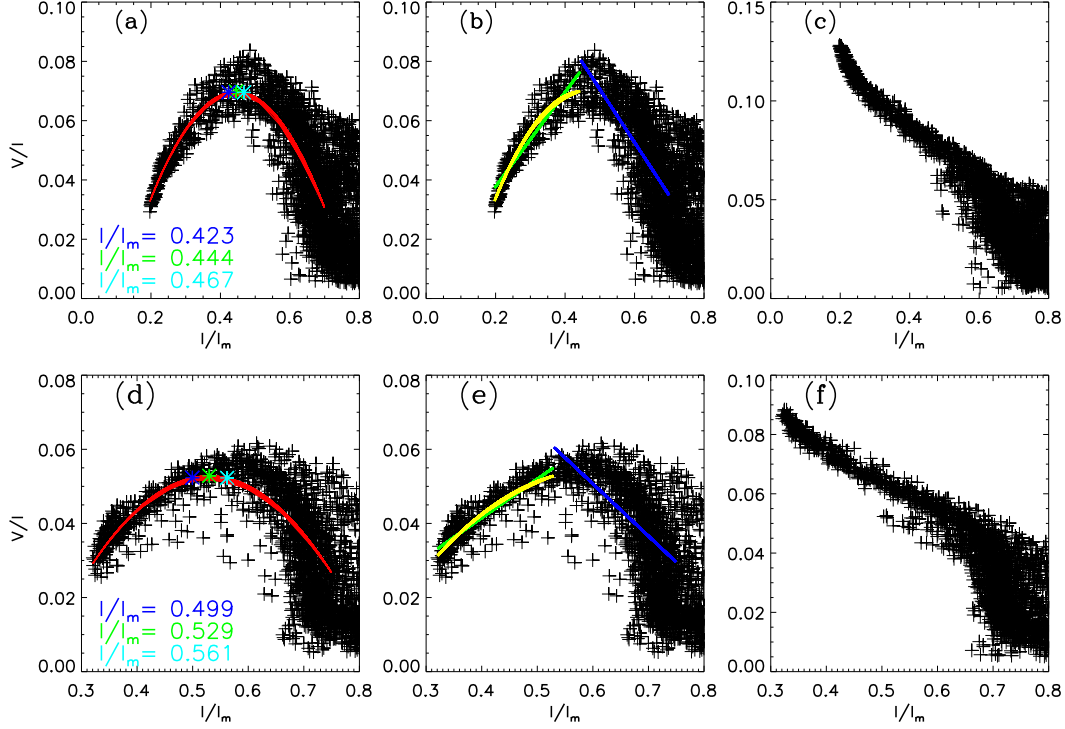


Fig. 4: Scatter plots of $|V/I|$ vs I/I_m for NOAA12158 (panels (a)–(c)) and NOAA12305 (panels (d)–(f)). The green asterisks in panels (a) and (d) present the apex of the second-order polynomial fit (red line). The cyan and blue asterisks present the $\pm 1\sigma$ uncertainty of apex. The corresponding I/I_m values are marked using the same color as those asterisks. The green and blue (yellow) lines are the linear (the second-order polynomial) fit to the data in panels (b) and (e). Panels (c) and (f) show the scatter plots of $|V/I|$ vs I/I_m after correcting magnetic saturation.

that the proposed correction method for saturation in B_L^{SMFT} is also effective for activity region includes multi-sunspots.

We performed such pixel by pixel comparison for 9 ARs and listed the correlation coefficients in Table 2. The correlation of B_L^{SMFT} and B_L^{HMI} is much better after eliminating magnetic saturation in B_L^{SMFT} . So the detection and correction algorithms can be used to re-calibrate the longitudinal magnetic field in strong field region observed by SMFT.

5 TESTING FOR LARGE SAMPLE

The algorithm was proved to be completely effective by comparing the results with HMI data for individual active region. To check the applicability of the algorithm for large sample, we tested it with 175 longitudinal magnetograms of 175 ARs observed in 2013 by SMFT. The magnetic saturation generally occurs in strong field region. Considering this actual situation, we set the following restrictions:

- (1) Only pixels where $|V/I| > 0.02$ and $I/I_m \leq 0.7$ are used for second-order polynomial fitting.
- (2) To ensure the rationality of the fitting result, we set $I_{min} < I_0 < 0.7$. I_{min} is the minimum value of I/I_m . If considering 1σ error range, we can set $I_{min} < I_{-\sigma} < I_0 < I_{+\sigma} < 0.75$.

42 ARs were detected with magnetic saturation. By **manual testing**, the detected ARs are all correct.

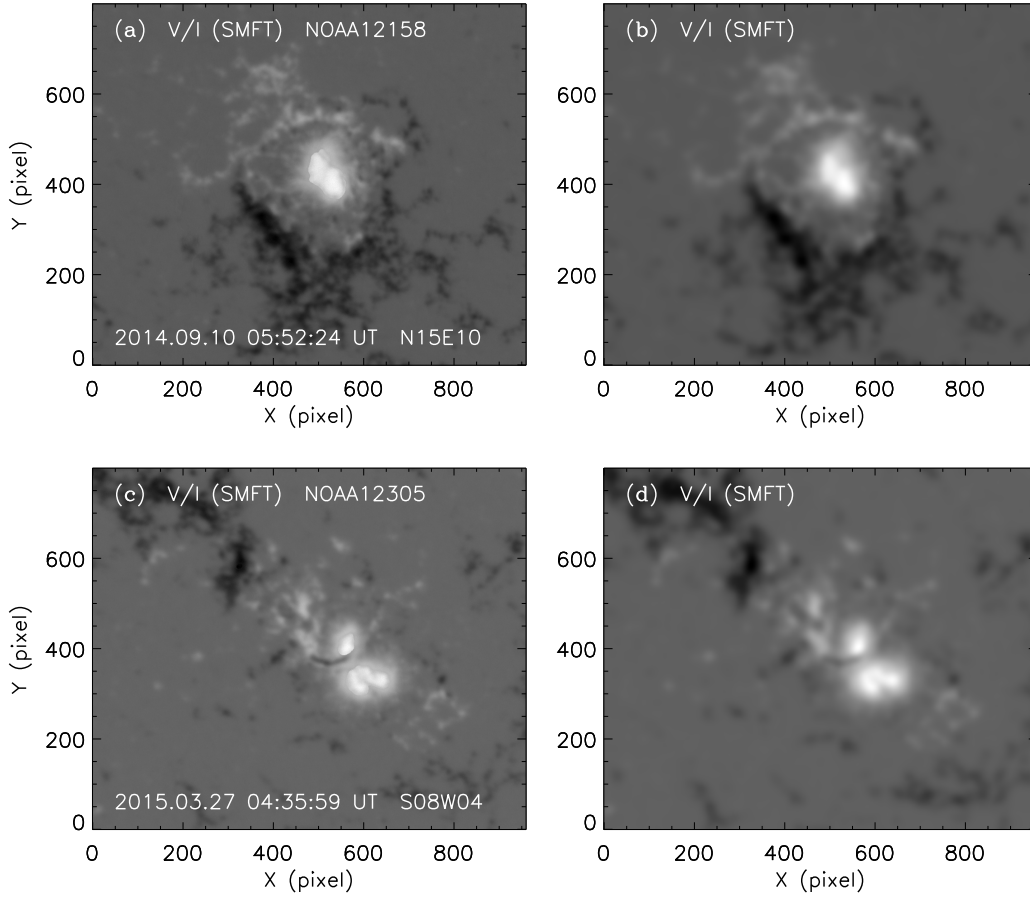


Fig. 5: Maps of Stokes V/I after correcting magnetic saturation for NOAA12158 (panels (a) and (b)) and NOAA12305 (panels (c) and (d)). The data in panels (b) and (d) are preprocessed with Gauss-smooth.

Table 2: Correlation coefficient of B_L for 9 ARs observed by SMFT and HMI

NOAA	Date	Position	C.C (before)	C.C (after)
11658	2013.11.19	S11W10	0.79	0.94
11899	2013.11.16	N06W03	0.84	0.93
11960	2014.01.25	S14E01	0.89	0.95
12027	2014.06.07	N13W01	0.85	0.95
12055	2014.05.12	N10W02	0.79	0.93
12149	2014.08.27	N10E11	0.88	0.94
12158	2014.09.10	N15E10	0.86	0.96
12305	2015.03.27	S08W04	0.88	0.96
12325	2015.04.19	N04E02	0.88	0.94

Notes: C.C (before) and C.C (after) represent the linear **correlation** coefficient before and after correcting magnetic saturation in B_L^{SMFT} , respectively.

$\sim 99.4\%$. If we adjust I/I_m range, the above undetected AR can also be detected. It is found that magnetograms of 5 ARs (**the total is 42**) were wrong after correcting saturation effect, which indicates that the accurate rate of correction is $\sim 88\%$. These 5 ARs are **either** relatively small or with projection effect. The

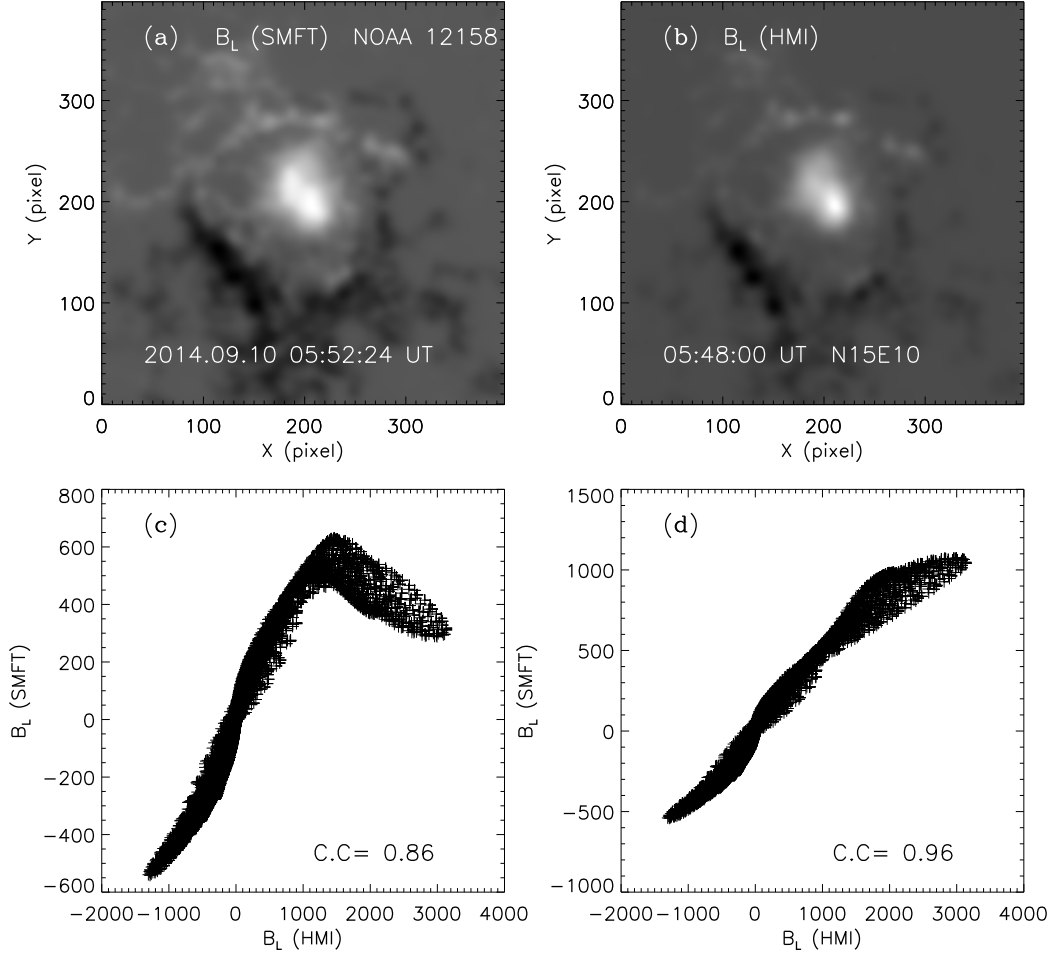


Fig. 6: Panels (a) and (b) are B_L maps of NOAA 12158 observed by SMFT and HMI, respectively. Panels (c) and (d) present the scatter plots of B_L observed by SMFT and HMI. The data taken by SMFT have saturation in (c) and no saturation in (d). C.C is the linear correlation coefficient.

6 CONCLUSIONS AND DISCUSSIONS

We developed an automatic detection and correction algorithms for saturation in longitudinal magnetic field observed by SMFT based on the relationship between Stokes V/I and I . It works well found in comparison with HMI data in case and sample study. The correlation of longitudinal magnetic fields between SMFT and HMI increased significantly after **correcting for** saturation effect. The accurate rate of detection and correction is $\sim 99.4\%$ and $\sim 88\%$ respectively. There are total 43 out of 175 ARs with saturation effect. It means 75.4% ARs don't need to correct saturation effect.

We didn't correct the scatter light when built the I - V/I relationship. The measured polarization signals are contaminated by scatter light (I_s). E.g., if we consider the scatter light, the equation 2 will be written as follow:

$$\frac{V}{I} = \frac{V_l - V_r}{V_l + V_r - 2I_s} \quad (5)$$

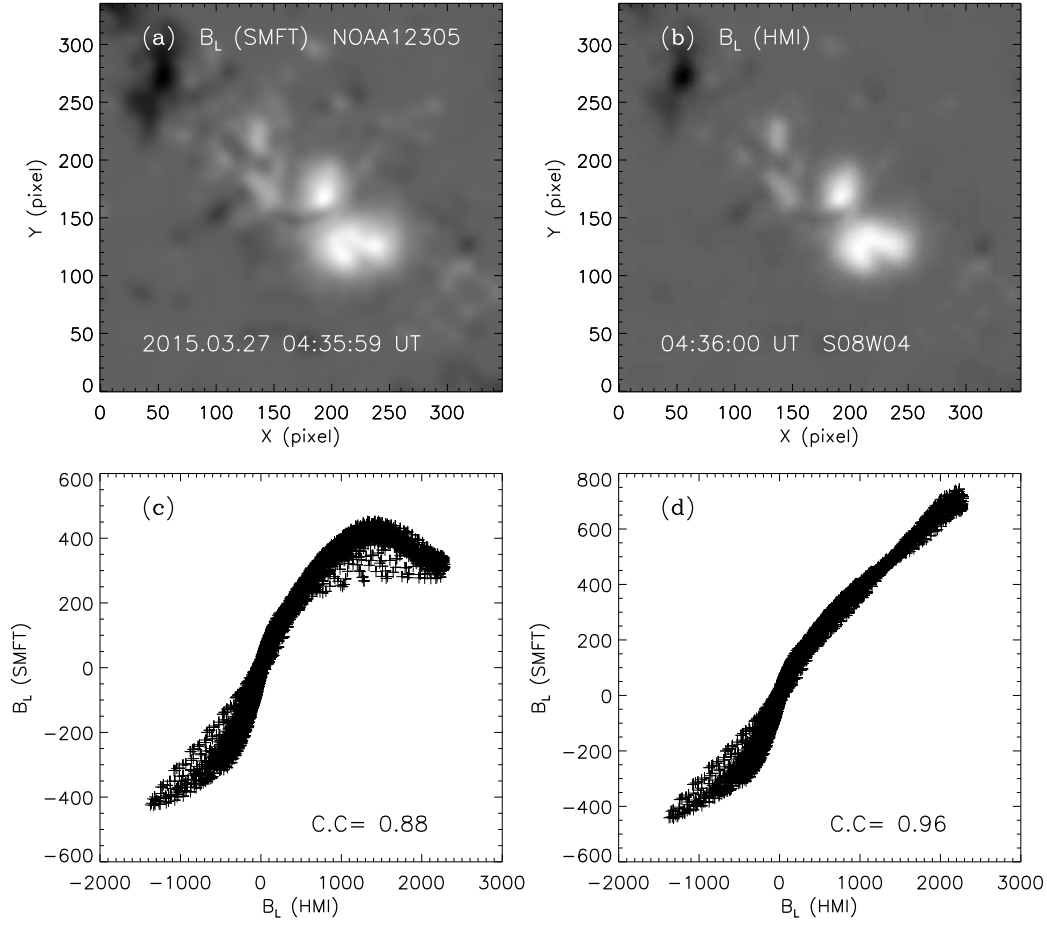


Fig. 7: Similar as Figure 6, but for NOAA12305.

Generally, I_s is determined at the solar limb. Here, we estimate I_s using the intensity in quiet sun (a certain percent of I_c). We took NOAA 12158 as an example to estimate the effect of the scatter light on the method. The result is shown in Figure 8. V/I in the umbrae increasing with larger scatter light is subtracted from the observed data. When the contamination level is lower than 8% (Figure 8(a)-(d)), the Stokes V/I vs I/I_m curves are very similar and the areas of saturation are almost the same although the threshold of saturation is different. It may be due to the normalized I/I_m being used. The saturation area decreases and the V/I vs I/I_m curve is close to linear when the contamination level is around 8% (Figure 8(e) and (f)), which shows that the measured polarized signals are likely affected more serious by scatter light than magnetic saturation. The above estimations indicate that the proposed method will not be affected by scatter light when the contamination level is lower, and the scatter light can be corrected as a magnetic saturation effect.

One advantage of this method is that it can calculate the threshold of saturation and correct it automatically. Therefore, this method can be used for the routine longitudinal field observations. Another advantage is that the used data **acquired** by one instrument which avoids a systematic error caused by cross-comparison. Especially, it can be used to correct the saturation effect in longitudinal magnetic fields

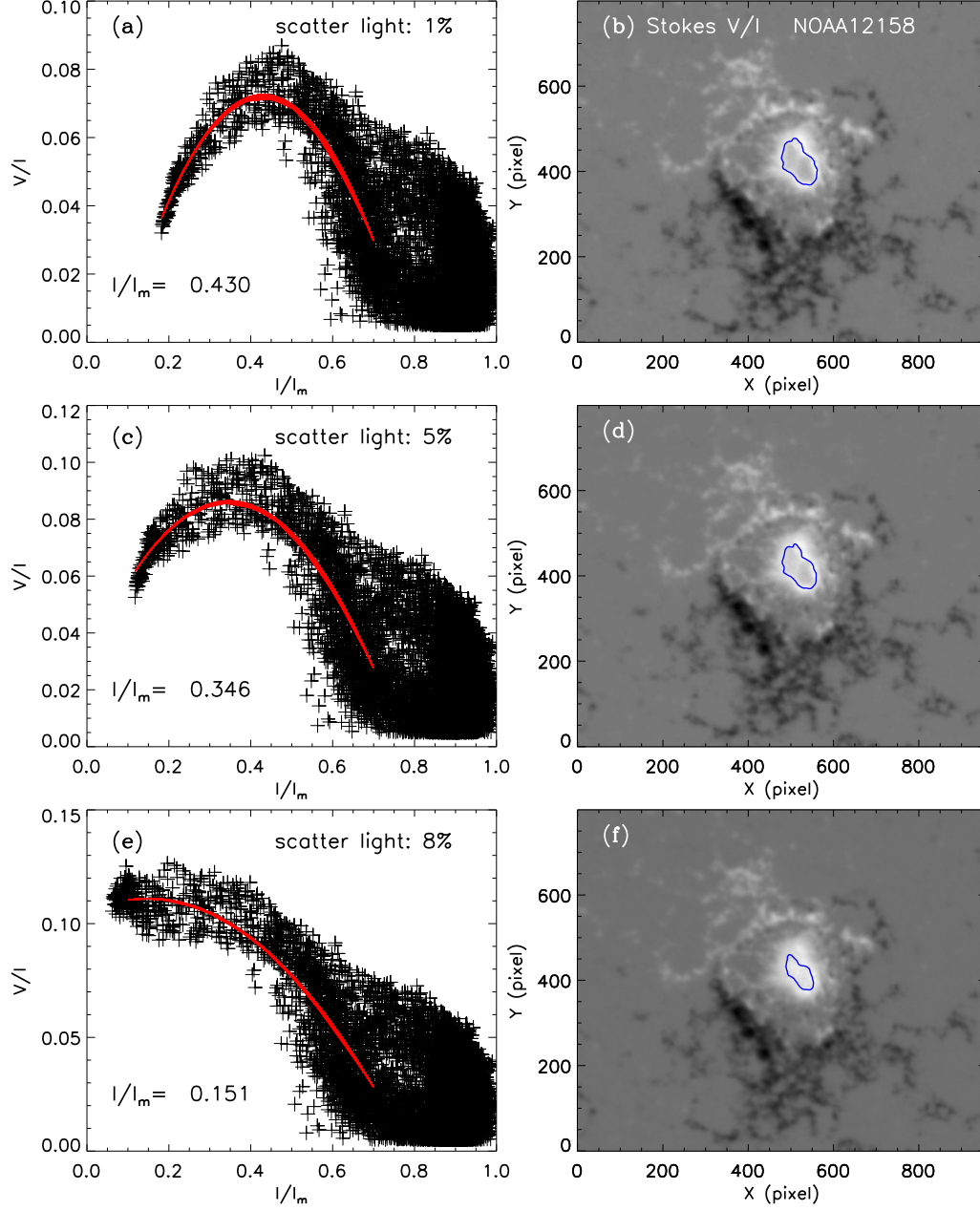


Fig. 8: **Scatter plots of $|V/I|$ vs I/I_m and V/I maps. (a) and (b): $I_s = I_c \times 1\%$. (c) and (d): $I_s = I_c \times 5\%$. (e) and (f): $I_s = I_c \times 8\%$. In panels (a), (c) and (e), the red line is the second-order polynomial fit and the marked I/I_m corresponds to apex. The blue contours in V/I maps represent the I/I_m apices marked in panels (a), (c) and (e).**

that the correction for saturation is not very accurate when the active regions are far from disk center. This may be caused by the projection effect. We will improve the method by considering the projection effect in future.

Acknowledgements This work is supported by National Natural Science Foundation of China (NSFC) under No. 11703042, 11911530089, U1731241, 11773038, 11427901, 11427803, 11673033, U1831107,

under No. XDA15320302, XDA15052200, XDA15320102, the 13th Five-year Informatization Plan of Chinese Academy of Sciences (Grant No. XXH13505-04). We acknowledge the use of data of SMFT/HSOS and HMI/SDO.

References

- Ai, G. X., Li, W., & Zhang, H. Q. 1982, *Acta Astronomica Sinica*, 23, 39 [2](#)
- Ai, G. X., & Hu, Y. F. 1986, *Acta Astron. Sinica*, 27, 173 [2](#)
- Bai, X.Y., Deng, Y.Y., Teng, F., et al. 2014, *MNRAS*, 445, 49. [2](#)
- Chae, J., Moon, Y.-J., Park, Y.-D., et al. 2007, *PASJ*, 59, S619 [2](#)
- Deng, Y. Y., Zhang, H. Y., Yang, J. F., et al. 2019, *Research in Astron. Astrophys. (RAA)*, 19, 157 [3](#)
- Gan, W. Q., Zhu, C., Deng, Y. Y., et al. 2019, *Research in Astron. Astrophys. (RAA)*, 19, 156 [3](#)
- Guo, J. J, Bai, X. Y., Deng, Y. Y., et al. 2020, *Sol. Phys.*, 295, 5 [2](#)
- Hale, G. E. 1908, *ApJ*, 28, 315 [1](#)
- Kosugi, T., Matsuzaki, K., Sakao, T., et al., *Sol. Phys.*, 243,3 [2](#)
- Leonard, T., & Choudhary, D. P. 2008, *Sol. Phys.*, 252, 33 [4](#)
- Liu, Y., Nortion, A.A., & Scherrer, P.H. 2007, *Sol. Phys.*, 241, 185 [2](#)
- Martínez, V., & Vázquez, M. 1993, *A&A*, 270, 494 [4](#)
- Moon, Y.-J., Kim, Y.-H., Park, Y.-D., et al. 2007, *PASJ*, 59, S625 [2](#), [5](#)
- Norton, A.A.,& Gilman, P.A. 2004, *ApJ*, 603, 348 [4](#)
- Plotnikov, A., Kutsenko, A. Yang, S. B., et al. 2019, eprint arXiv:1904.07081 [3](#)
- Schou, J., Borrero, J. M., Norton, A. A., et al. 2012, *Sol. Phys.*, 275, 327 [2](#)
- Su, J. T., Bai, X. Y., Chen, J., et al. 2019, *Research in Astron. Astrophys. (RAA)*, 19, 161 [3](#)
- Su, J. T., & Zhang, H. Q. 2004, *ChJAA (Chin. J. Astron. Astrophys.)*, 4, 365 [2](#), [7](#)
- Svalgaard, L., Duvall, T.L., Jr., & Scherrer, P.H. 1978, *Sol. Phys.*, 58, 225 [2](#)
- Ulrich, R.K., Evans, S., Boyden, J.E., et al. 2002, *Astrophys. J. Suppl.* 139, 259 [2](#)
- Wang J. X., Shi Z. X., Wang H. N., et al. 1996, *ApJ*, 456, 861 [2](#)
- Zhang, H. Q. 2019, *Sci. China-Phys. Mech. Astron.*, 4, 365 [2](#)